RSC Sustainability

ROYAL SOCIETY OF CHEMISTRY

PAPER

View Article Online
View Journal | View Issue



Cite this: *RSC Sustainability*, 2024, **2**, 2669

# Multilayered frequency-selective and high-performance electromagnetic interference shielding materials derived from waste polyurethane foam†

Jian Zhang,[ac] Qunhao Wang,[a] Zehang Zhou,[a] Zengyan Sui,[a] Chao Wang*[b] and Canhui Lu*[a]

The development of electromagnetic interference (EMI) shielding composites with tunable frequency-selective shielding attributes is of critical importance for their applications in military and signal detection fields. This study introduces a multilayered conductive polymer composite comprising waste polyurethane foam (WPUF), ground tire rubber (GTR) powders, carbon nanotubes (CNTs) and cellulose nanofibres (CNFs). The bulky waste polymeric material with a porous structure, WPUF, is utilized as the substrate to construct the rationally designed alternative conductive-insulating multilayered structure, which significantly enhances the multiple-reflection of the incident EM wave. This conductive composite provides enhanced EMI shielding effectiveness and unique tunable frequency-selective EM shielding performance. The EMI shielding peak shifts with the variation of CNTs, and adjusting the GTR/WPUF ratio in the insulating layer enables fine-tuning of its selective EMI shielding performance over a specific frequency range. In addition, the composite demonstrated robust durability, which benefits its practical application. This approach proposes a practical and innovative method for the design and fabrication of advanced frequency-selective EMI shielding composites with bulky polymer wastes.

Received 18th April 2024
Accepted 25th July 2024

DOI: 10.1039/d4su00181h

rsc.li/rscsus



### Sustainability spotlight

Waste Polyurethane Foam (WPUF) is a by-product of various consumer and industrial applications, including furniture, insulation, and automotive components. The disposal of WPUF poses significant environmental challenges, primarily due to its non-biodegradable nature and the release of toxic compounds upon incineration. The recycling and reuse of WPUF is important for environmental sustainability and resource conservation. Herein, WPUF is employed as a porous 3D substrate for the deposition of carbon nanotubes and insulating the separator to construct the conductive/insulating alternative multilayered structure of electromagnetic interference shielding materials, providing sustainable and value-added utilization of the representative bulky waste. This study aligns with the UN's Sustainable Development Goals 11 (Sustainable Cities and Communities) and 12 (Responsible Consumption and Production).

## Introduction

The widespread use of mobile and wearable devices has raised an increasingly serious electromagnetic interference (EMI) pollution problem,[1–9] which presents a significant threat to precision instruments, information security and even human health.[10–13] The development of lightweight yet high-performance EMI shielding materials is crucial to meet the demands of modern industrial and commercial applications.[14–17] Conductive polymer composites (CPCs) have attracted extensive research interest due to their versatility, light weight, flexibility, durability, and adjustable characteristics.[18,19] The conductivity of CPCs is of pivotal importance in determining their EMI shielding effectiveness (EMI SE).[6,20] However, the excessive use of a conductive filler compromises the other critical aspects including cost, flexibility, machinability, and mechanical reliability of the composite material.[8] Developing high-performance polymer-based EMI shielding materials with favourable flexibility and mechanical properties remains a significant challenge.[21–23]

Optimizing the structural design of CPCs emerges as a feasible approach to minimize the requisite volume of the

[a]*State Key Laboratory of Polymer Materials Engineering, Polymer Research Institute at Sichuan University, Chengdu 610065, China. E-mail: canhuilu@scu.edu.cn; Fax: +86-28-85402465; Tel: +86-28-85460607*

[b]*National Engineering Research Centre for Synthesis of Novel Rubber and Plastic Materials, SINOPEC, Beijing Research Institute of Chemical Industry, Beijing 100013, China. E-mail: wangchao.bjhy@sinopec.com*

[c]*Fujian Provincial Key Laboratory of Environmental Engineering, Fujian Provincial Academy of Environmental Science, Fuzhou 350013, China*

† Electronic supplementary information (ESI) available. See DOI: https://doi.org/10.1039/d4su00181h

conductive filler while simultaneously enhancing its EMI shielding efficacy.[4,7,19,24,25] Sandwiched or multilayered structures are extensively studied for high-performance EMI shielding materials.[20,26,27] The enhancement of EMI shielding effectiveness is achieved through the designated distribution of conductive fillers across the conductive layers, increasing the effective filler concentration in certain regions to establish multiple electrically conductive pathways. Furthermore, this rationally designed structure enables the multiple reflections of incident EM waves at conductive interfaces, thereby contributing to the polarization and absorption losses of electromagnetic waves.[11,28–31] Consequently, multilayered CPCs can achieve enhanced EMI shielding performance with minimized conductive fillers.[32]

Intriguingly, multilayered CPCs with parallel interfaces facilitate the multiple reflections of incident EM waves between the parallel reflectors. This may lead to selective EMI shielding performance, which is likely attributable to the interference between reflected and incident electromagnetic waves.[33,34] In a previous report, Wang *et al.* prepared a flexible CPC with a sandwich structure using silicone rubber and graphene, presenting an average EMI SE value of 30.4 dB at low graphene content (3 wt%).[35] This unique electromagnetic shielding characteristic has potential applications in a variety of fields, including military and signal detection.[36–38]

Waste polyurethane foam (WPUF) is a by-product of various consumer and industrial applications, representing a typical bulky polymer waste. The majority of WPUF is typically discarded in landfills or incinerated, resulting in significant environmental contamination.[39,40] Previous studies have demonstrated that waste polyurethane foam can be combined with other materials to create composite materials with potential applications in sound absorption, EMI shielding, and infrared stealth.[41,42] Combined with the excellent structural stability of WPUF, it is anticipated that WPUF has the potential to be employed in the preparation of multilayered CPCs for EMI shielding. Moreover, the recycling and value-added reuse of WPUF represent a significant opportunity for advancing environmental sustainability.

In this study, waste polyurethane foam (WPUF) along with carbon nanotubes (CNTs), cellulose nanofibres (CNFs) and ground tire rubber (GTR) powder are employed to prepare flexible CPCs with a multilayered structure. Conductive WPUF/CNT/CNF (WCC) foam was prepared by depositing CNT/CNF onto three dimensional interconnected porous WPUF. The conductive WCC foam and the insulating WPUF foam were separately subjected to hot-pressing into thin foams, which were then laminated to form a composite denoted as WCC/WPUF (WCC/W). This composite material presents a distinctive interlayered structure, comprising an external conductive WCC layer and a central insulating WPUF layer. Its average EMI SE value could reach 39.9 dB at a low CNT content of 2.31 wt%, which is significantly higher than that of pure WCC with the same CNT content (27.2 dB). Impressively, this WCC4/W with a multilayered structure exhibited obvious frequency selectivity and stability, providing a novel strategy to achieve flexible EMI shielding materials with selective shielding capabilities.

## Experimental section

### Materials

The samples of flexible waste polyurethane foam (WPUF) were supplied by the Hongmiaoling Comprehensive Garbage Treatment Plant in Fuzhou (China), and were the leftover materials in the furniture packaging process. The samples of porous flexible polyurethane foams (PUF) were provided by Yuanli Shoe Material Co., Ltd in Quanzhou (China), and were the residual materials resulting from the manufacturing process. The pore size of the WPUF and PUF was in the range of 300–500 μm. Ground tire rubber (GTR) with a particle size of 10–250 μm was provided by Meiya Plastic Technology Co., Ltd, Jiangsu, China. Carbon nanotubes (CNTs) were provided by Organic Chemicals Co., Ltd, Chengdu, China. Commercial bleached filter paper was purchased from the Filter Paper Factory, Fushan, China. 2,2,6,6-Tetramethyl-piperidin-1-oxyl (TEMPO) was received from Sun Chemical Technology Co., Ltd, Shanghai, China. Sodium bromide (NaBr) was provided by Damao Chemical Reagent Co., Ltd, Tianjin, China. Sodium hypochlorite (NaClO), sulfuric acid ($H_2SO_4$), hydrochloric acid (HCl) and sodium hydroxide (NaOH) were all obtained from Kelong Reagent Co., Ltd, Chengdu, China.

### Fabrication of the WCC/W composite

The detailed preparation process of the CNT/CNF aqueous suspension is given in the ESI.† Initially, the WPUF was immersed in a CNT/CNF aqueous suspension for 30 min and then dried at 50 °C for 7 h to produce WCC*x* foams (*x* represents the number of soaking/drying cycles). Regulating the content of CNTs in WCC foams can be achieved by adjusting the soaking/drying cycles (Table S1†). WPUF and WCC*x* foams were compressed into a thin foam with a thickness of 1.0 mm under a pressure of 20 MPa at 160 °C. The obtained WCC*x* and WPUF thin foams were alternately stacked in layers, as shown in Fig. S1.† Then, the WCC*x*/WPUF (WCC*x*/W) composites were created by compression-molding the stack at 160 °C and 20 MPa. The CNT contents of WCC*x*/W composites are shown in Table S2.† For the control, 4 pieces of WCC4 thin foams were stacked and hot-pressed at 160 °C and 20 MPa to obtain the WCC4 composite.

The detailed fabrication process for WCC4/GTR (WCC4/G), WCC4/PUF (WCC4/P) and WCC4/GUR/PUF (WCC4/GP) composites is provided in the ESI.†

### Characterization

The morphologies of the as-prepared samples were characterized by SEM (Inspect F50, the Netherlands) at 20 kV. Electric conductivity of WCC was measured by using a Four-probe resistivity tester (HPS2661, China). EMI shielding properties of all samples were studied within the frequency range of the X-band (8.2–12.4 GHz) using an Agilent vector network analyser (N5247A, 10 MHz to 67 GHz, NASA Technologies, USA). The calculation of EMI shielding efficiency is provided in the ESI.†

## Results and discussion

Fig. 1a provides an intuitive illustration of the preparation process of the WCC/W composites, wherein WCC serves as the conductive layer, and WPUF acts as the insulating layer. The multilayered structure of WCC/W was obtained by the sequential stacking and hot pressing of the conductive and insulating layers. SEM was used to characterize the morphological structure of WCC/W. As illustrated in Fig. 1b and S2,† the original three-dimensional porous architecture of the WCC foam is significantly altered by the hot-pressing process, resulting in a tightly compacted composite structure. The CNTs were uniformly deposited on the surface of the WPUF skeleton (Fig. 1c), providing a stable conductive path for the WCC/W. Fig. 1d presents the cross-section SEM image of WCC/W. The stable mechanical properties of the WCC/W are guaranteed by the good bonding between the layers. The cross-sectional SEM image (Fig. 1d) highlights the stable mechanical integrity of the composite foam, which is attributed to the excellent interlayer adhesion.

Fig. S3† compares the conductivity of WCC films with different CNT loading cycles. The conductivity of the WCC1 film reaches 4.4 S $m^{-1}$, exceeding the threshold (1.0 S $m^{-1}$) required for commercial EMI shielding materials.[43,44] With the increase in CNT loading cycles, the conductivity of the WCC film is gradually improved, achieving a peak conductivity of 65.3 S $m^{-1}$ for WCC4. The superior electrical conductivity of WCC facilitates the enhancement of EMI shielding effectiveness.[45–47] The EMI SE of both the WCC4 film and WCC4/W composite is elucidated in Fig. 2(a and b), revealing a substantial enhancement in EMI SE for the WCC4/W composite, attributable to its multilayered structure. The WCC4 film presents an average EMI SE of 27.2 dB, whereas the WCC4/W composite with the same CNT content achieves an average EMI SE of 39.9 dB, significantly exceeding the commercial EMI shielding threshold of 20 dB.[48,49] Fig. 2b compares the shielding effectiveness related to reflection ($SE_R$) and absorption ($SE_A$) for both WCC4 and WCC4/W, indicating that $SE_A$ plays a predominant role in both samples. The $SE_A$ of WCC4/W has an obvious EMI shielding peak in the X-band, while the $SE_A$ of WCC4 has no obvious EMI shielding peak. This result demonstrates that the unique structure of WCC/W predominantly enhances the absorption of the EM wave. Furthermore, the absorption coefficient ($A$), reflection coefficient ($R$) and transmission coefficient ($T$) of WCC4/W are calculated (Fig. S4†). The average $T$-value is close to 0, indicating that the incident EM wave is almost completely blocked by WCC4/W.[50,51] In addition, the average value of $A$ (0.80) is significantly higher than that of $R$ (0.20), indicating that the WCC/W composite adheres to an absorption-dominated EMI shielding mechanism.[44,52–54]

Interestingly, compared to the WCC4 film, the WCC4/W composites exhibit pronounced selective EMI shielding performance. The EMI SE of WCC4/W exhibits a significant EMI shielding peak of 46.6 dB at a frequency of 10.5 GHz

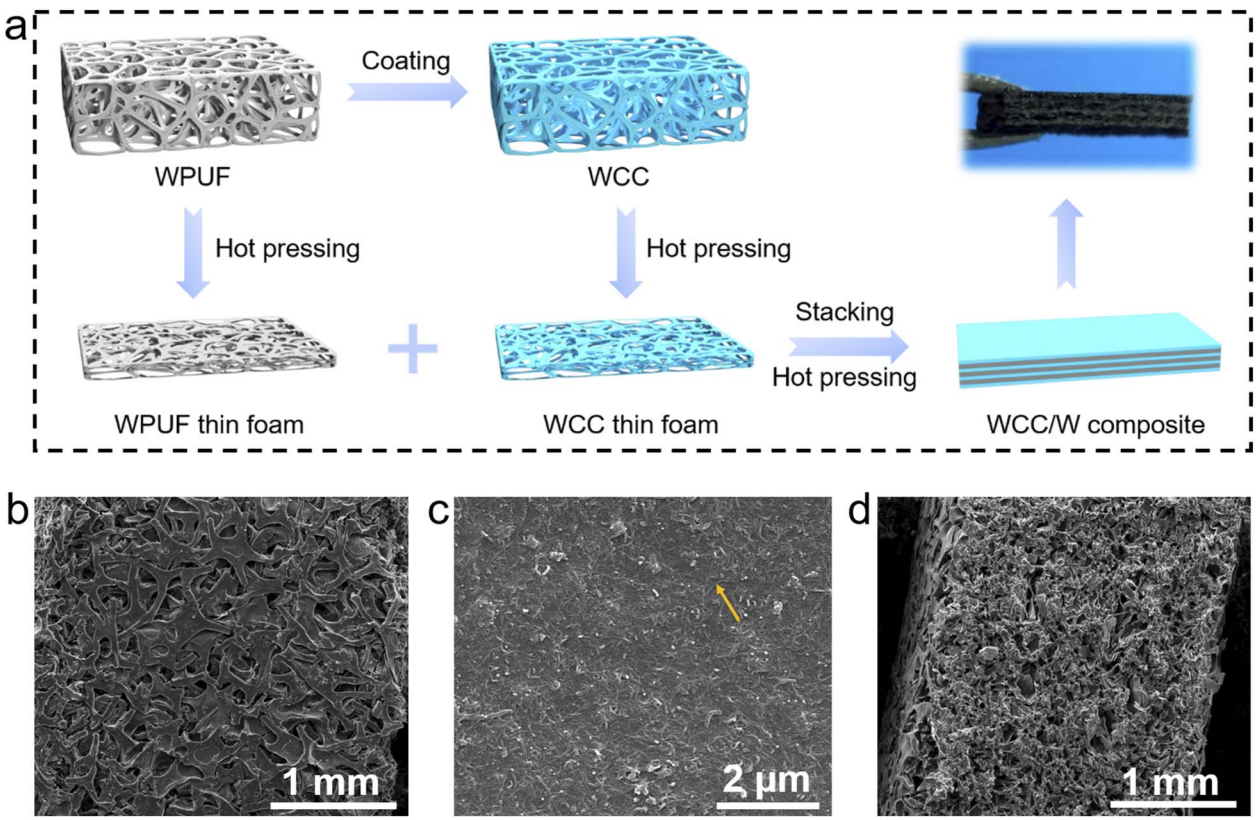


Fig. 1 (a) Schematic diagram of the preparation process of the WCC/W composites. (b and c) Surface SEM and (d) cross-section SEM images of WCC/W.

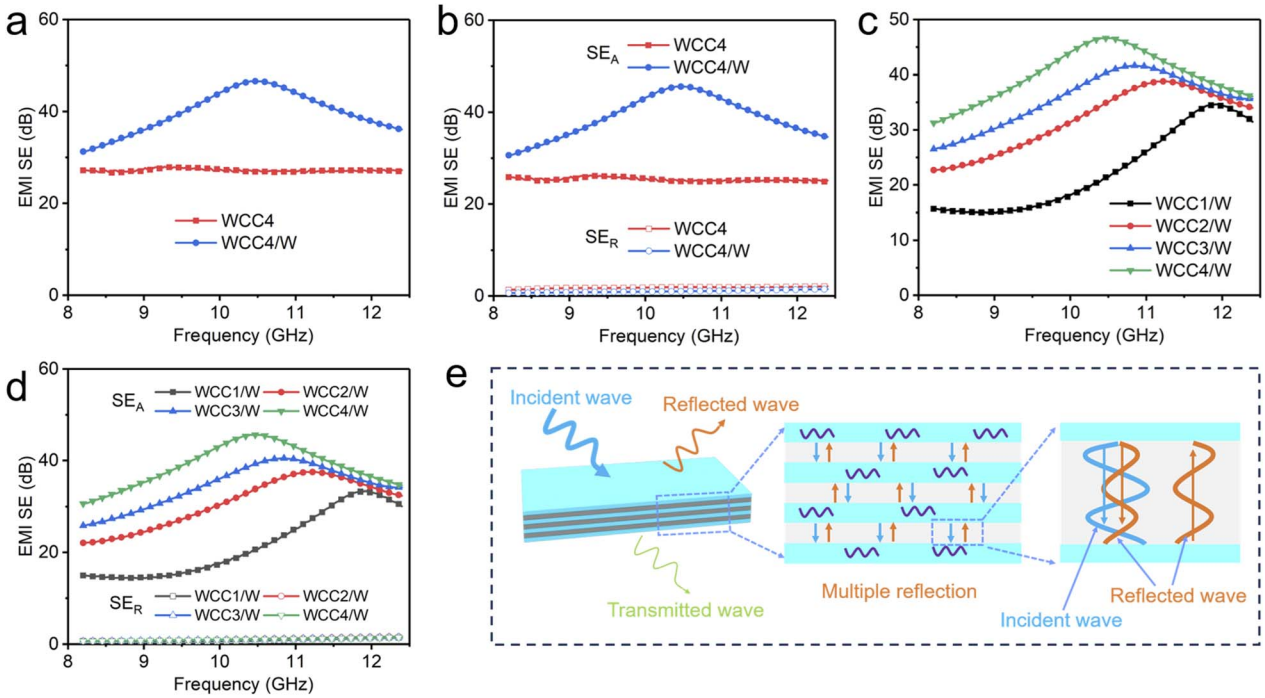


Fig. 2 (a) EMI SE for the WCC4 film and WCC4/W composite. (b) Variation of $SE_R$ and $SE_A$ for the WCC4 film and WCC4/W composite. (c) EMI SE and (d) variation of $SE_R$ and $SE_A$ for WCC/W composites. (e) Schematic illustration of the EMI shielding mechanism of WCC/W composites.

(Fig. 2a), which is significantly higher than the average EMI SE value of 39.9 dB. The EMI SE of WCC/W composites with varying CNT contents is shown in Fig. 2(c and d). The increase in the CNT content results in a rise of the average EMI SE value from 22.5 dB of WCC1/W to 39.9 dB. Additionally, the EMI shielding peak shifts from 11.9 GHz for WCC1/W to 10.5 GHz for WCC4/W. The observed frequency selectivity is consistent with the trend of $SE_A$ values for WCC/W composites (Fig. 2b and d). Furthermore, a WCC4/W composite with a thickness of 1 mm was prepared in accordance with the preparation method for the WCC4/W composite (2 mm), but the thickness of each layer reduced by half. As shown in Fig. S5,† the WCC4/W composite (1 mm) also exhibits pronounced selective EMI shielding performance, with a reduction in the maximal EMI SE peak from 46.6 dB (2 mm) to 34.2 dB (1 mm). The frequency of the EMI shielding peak is also subject to change in accordance with the thickness, which is consistent with the early studies. The underlying EMI shielding mechanism of the WCC/W composite with a multilayered structure is elucidated in Fig. 2e. The highly conductive WCC layer in WCC/W composites might experience an impedance mismatch effect due to the abundance of free electrons, leading to the interaction of reflected EM waves with the electron carriers in the conductive network of the WCC layer,[10] engendering considerable EM wave attenuation.[55–58] Residual EM waves traverse the surface WCC layer and subsequently penetrate the insulating WPUF layer. Compared to the transition in a pure WCC film, the intermediate layer of WPUF provides parallel space for multiple reflections of EM waves, which extends the propagation path of EM waves in the WCC layer and further facilitates EM wave attenuation.[5,59,60] Note that the electromagnetic waves that have undergone two reflections exhibit the same frequency and direction as the incident electromagnetic waves. This phenomenon will result in the interference of electromagnetic waves, with the interference effect dependent on the phase difference between the electromagnetic waves. When a suitable phase difference is present, the intensity between the electromagnetic waves will be offset, thereby increasing the electromagnetic wave loss. In the same sample, the phase difference is correlated with the frequency of the electromagnetic wave. Therefore, the WCC/W composites exhibit varying EMI shielding effectiveness across different frequency ranges, resulting in the characteristics of frequency-selective EMI shielding. In this structure, incident EM waves undergo multiple reflections between the parallel conductive layers (Fig. 2e).[20,35,61] The interaction between these multiply reflected waves and the incident wave amplifies EM wave dissipation at specific frequencies. Consequently, the absorption of EM waves at these frequencies is markedly elevated compared to others, thereby imparting the WCC/W composites with notable frequency-selective EMI shielding effectiveness.

The frequency range of selective shielding is modulated by varying the concentration of the conductive filler in the conductive layer (Fig. 2c). However, the average EMI SE value of the composite also undergoes alteration in response to alterations in the conductive filler content, thereby presenting a challenge in accurately adjusting the selective EMI shielding frequency range without affecting the overall EMI SE. Different

materials (GTR, WPUF and PUF) are used as insulation layers to investigate how to achieve frequency selectivity without changing the overall EMI SE. As shown in Fig. 3a, GTR powder, WPUF foam and PUF foam (see Fig. S6(a–c)† for the photographs) are hot pressed into thin films, respectively. Then, they are integrated with conductive WCC4 thin foam to fabricate multilayered composites denoted as WCC4/G, WCC4/W, and WCC4/P, based on the insulating layer used. The cross-sectional SEM images of WCC4/G, WCC4/W and WCC/P presented in Fig. S6(d–f)† reveal that there is an absence of noticeable stratification among the layers, demonstrating robust interlayer adhesion within the composites.

The EMI SE of WCC4/G, WCC4/W and WCC4/P composites is presented in Fig. 3b–d. WCC4/G, WCC4/W and WCC4/P with various insulation layers exhibit significant EMI shielding frequency selectivity. The average EMI SE values are approximately 40.4 dB, 39.9 dB and 37.1 dB, respectively, indicating their substantial EMI shielding performance. Impressively, each sample presents distinctive selective shielding frequency ranges, characterized by EMI shielding peaks at 11.85 GHz for WCC4/G, 10.47 GHz for WCC4/W, and 9.02 GHz for WCC4/P, respectively. In addition, the peak EMI SE values across these samples display minimal variance. Fig. 3c and d demonstrate that altering the insulating layer types in a multilayered structure could adjust the frequency range of electromagnetic wave absorption. The frequency-selective EMI shielding performance is achieved without compromising the overall EMI SE.

Fig. 3e depicts the EMI shielding mechanism of the EM waves with identical frequencies traversing different interlayers within the composite structure. The electromagnetic

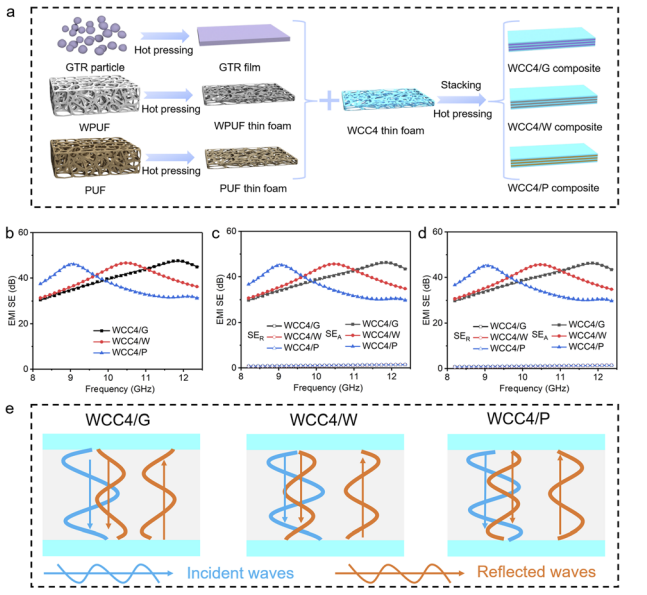


Fig. 3 (a) Schematic diagram of the preparation process of the WCC4/G, WCC4/W and WCC4/P composites. (b) EMI SE and variation of (c) $SE_A$ and (d) $SE_R$ for WCC4/G, WCC4/W and WCC/P composites. (e) Schematic illustration of the EMI shielding mechanism of the same frequency electromagnetic wave in different interlayers.

EM waves propagate at different speeds in different media, leading to the variation of their wavelength across different interlayers, as determined by the calculation formula for EM wave velocity ($v = f\lambda$), where $v$ represents the velocity, $f$ represents the frequency, and $\lambda$ represents the wavelength. Fig. 3e shows that EM waves with a specific wavelength achieve the optimal interference effect within interlayer 1. This promotes the attenuation of electromagnetic waves, manifesting as pronounced EMI shielding peaks within the frequency range corresponding to this wavelength. However, the wavelength is not optimal for the interference effect in interlayers 2 and 3. For the composites with a fixed structure and conductive layer, the wavelength corresponding to the EMI shielding peak remains constant. Therefore, the position of the frequency band corresponding to the EMI shielding peak is intrinsically linked to the propagation speed of the EM wave in the insulation layer. Consequently, modulation of the frequency location of the EMI shielding peak can be achieved through the adjustment of the insulating layer material. This methodology provides a viable approach for the customisation of frequency-selective EMI shielding properties.

This study further investigates the strategic manipulation of the EMI shielding peak position. As shown in Fig. 4a, WCC4 is employed as the outer conductive layer while the insulation layer comprises a combination of GTR and WPUF, contributing to selective shielding efficacies in higher and lower frequency domains, respectively. The fabricated composites are named WCC4/GP1, WCC4/GP2 and WCC4/GP3 according to the different GTR/PUF weight ratios (2 : 1, 1 : 1 and 0.5 : 1). GTR and PUF skeletons are evenly distributed within the pores of the PUF skeleton, ensuring the structural stability of the intermediate layer (Fig. S7†).

Fig. 4b–d reveal the comparison of the EMI SE of WCC4/G, WCC4/GP and WCC4/P composites. WCC4/GP1, WCC4/GP2 and WCC4/GP3 exhibit pronounced frequency selectivity in their EMI shielding performance. The selected shielding frequency ranges of the three samples are situated between the EM shielding peaks of WCC4/G and WCC4/P. With the increase in PUF content, the EMI shielding peak gradually shifts towards lower frequencies. Specifically, the shielding peaks for WCC4/GP1, WCC4/GP2, and WCC4/GP3 are located at approximately 11.08 GHz, 10.55 GHz, and 9.36 GHz, respectively. Thus, modifying the GTR/PUF ratio in the sandwich can effectively regulate the selective EMI shielding frequency range of the WCC4/GP composite. These findings have significant potential implications for the design and fabrication of frequency-selective EMI shielding materials.

Moreover, an optimal EMI shielding material necessitates robust durability in practical applications.[62] Fig. S8† shows that the WCC4/G, WCC4/W, and WCC4/P composites all exhibit notable flexibility, high tensile strength (>4 MPa) and certain stretchability. These excellent mechanical properties assist in maintaining stable EMI shielding properties when subjected to external forces. Fig. 5a presents the EMI shielding performance of WCC4/G, WCC4/W and WCC/P composites after repeated deformation. It can be observed that the EMI SE remains

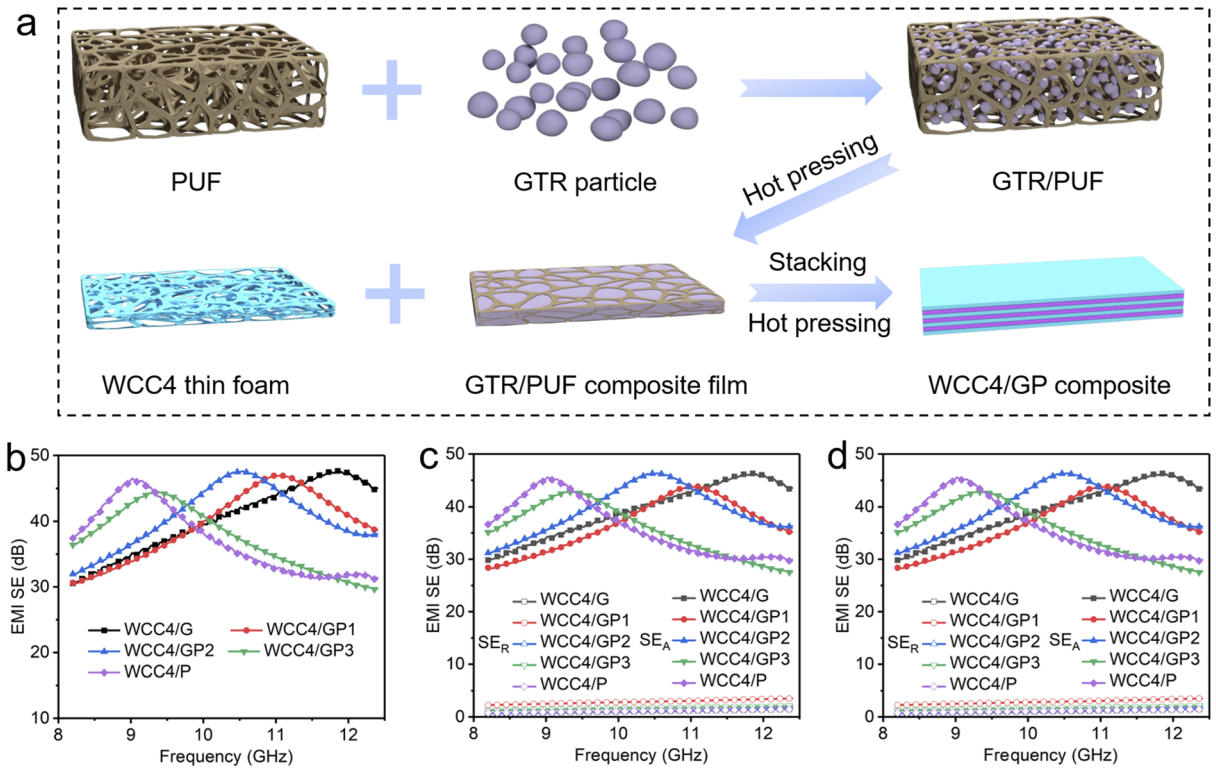


Fig. 4 (a) Schematic diagram of the preparation process of the WCC4/GP composites. Variation of (b) EMI SE, (c) SEA and (d) SER for WCC4/G, WCC4/GP and WCC/P composites.

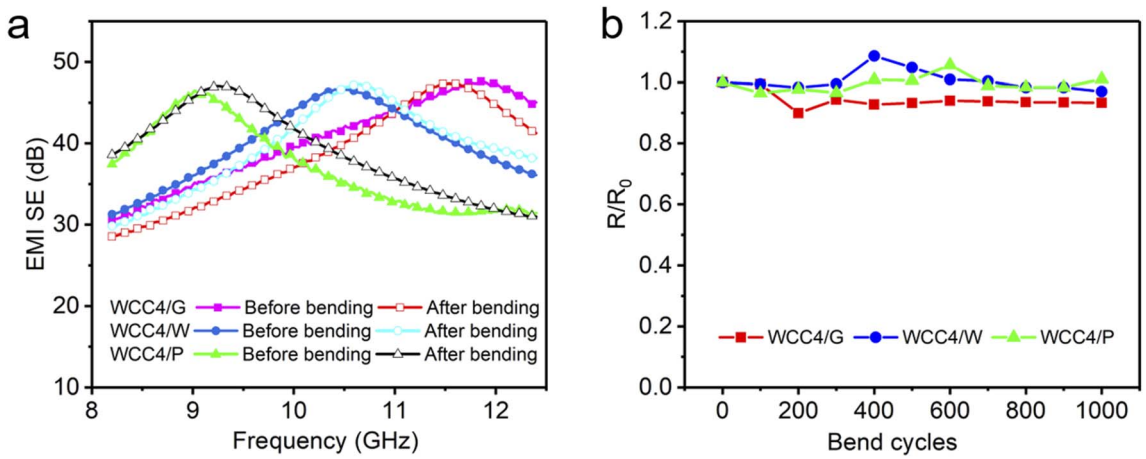


Fig. 5 (a) EMI SE for WCC4/G, WCC4/W and WCC4/P composites before and after bending for 1000 cycles, respectively. (b) The normalized resistance ($R/R_0$) of WCC4/G, WCC4/W and WCC4/P composites as a function of bending cycles, respectively.

consistent with the initial value even after 1000 bending cycles. Notably, the position, intensity and contour of the EMI shielding peak showed no significant changes, indicating the exceptional stability of the composites. The variation of electrical resistance ($R/R_0$) could be employed to quantitatively reveal the impact of the multilayered structures against repeated mechanical deformation.[30] Fig. 5b presents the normalized $R/R_0$ of WCC4/G, WCC4/W and WCC/P composites as a function of bending cycles. All the $R/R_0$ values remain stable even after 1000 bending cycles, further indicating great potential as excellent EMI shielding materials.

## Conclusions

This work provides a novel strategy to manufacture flexible CPCs with frequency-selective EMI shielding performance. The WCC/W composites exhibited exceptional EMI shielding performance, achieving an average EMI SE of 39.9 dB at a low

CNT content (2.31 wt%) with a thickness of 2 mm. The rationally designed alternative conductive-insulating multilayered structure leads to the Fabry–Perot cavity effect, contributing to the pronounced frequency-selective EMI shielding performance. Moreover, it was observed that an increase in the concentration of CNTs within the conductive WCC layer resulted in enhanced electrical conductivity of the composite, accompanied by a downward frequency shift of the EMI shielding peak. The position of the EMI shielding peak could be modulated without compromising the overall EMI shielding performance by the modification of the insulating layer. In addition, the composite demonstrated good durability against repeated deformation.

## Data availability

The data supporting this article have been included as part of the ESI.†

## Conflicts of interest

There are no conflicts to declare.

## Acknowledgements

This work was supported by the Sinopec Group Key R&D Project (222053), the National Natural Science Foundation of China (51861165203), the Sichuan Science and Technology Program (2020YJ0261 and 2019YJ0125), the State Key Laboratory of Polymer Materials Engineering (sklpme2019-2-19), the Special Foundation for Innovation-Driven Development of Hezhou (Hekechuang PT0710004), and the Opening Project of Guangxi Key Laboratory of Calcium Carbonate Resources Comprehensive Utilization (HZXYKFKT201902).

## Notes and references

1 B. Li, N. Wu, Y. Yang, F. Pan, C. Wang, G. Wang, L. Xiao, W. Liu, J. Liu and Z. Zeng, *Adv. Funct. Mater.*, 2023, **31**, 2213357.
2 J. Yang, H. Wang, Y. Zhang, H. Zhang and J. Gu, *Nano–Micro Lett.*, 2024, **16**, 31.
3 X. Li, X. Sheng, Y. Fang, X. Hu, S. Gong, M. Sheng, X. Lu and J. Qu, *Adv. Funct. Mater.*, 2023, **33**, 2212776.
4 X. Y. Wang, S. Y. Liao, Y. J. Wan, P. L. Zhu, Y. G. Hu, T. Zhao, R. Sun and C. P. Wong, *J. Mater. Chem. C*, 2022, **10**, 44–72.
5 Y. Zhang and J. Gu, *Nano–Micro Lett.*, 2022, **14**, 89.
6 Y. Zhang, K. Ruan, K. Zhou and J. Gu, *Adv. Mater.*, 2023, **35**, 2211642.
7 Y. Chen, Y. Yang, Y. Xiong, L. Zhang, W. Xu, G. Duan, C. Mei, S. Jiang, Z. Rui and K. Zhang, *Nano Today*, 2021, **38**, 101204.
8 L. Wang, Z. Ma, Y. Zhang, L. Chen, D. Cao and J. Gu, *SusMat*, 2021, **1**, 413–431.
9 J. Zhang, Q. Wang, B. Huang, X. Xue, M. Li, W. Zhang and C. Lu, *Ind. Eng. Chem. Res.*, 2022, **61**, 13083–13091.
10 J. Zhang, Q. Wang, X. Xue, M. Li, X. Sun, J. Zhao, W. Zhang and C. Lu, *Composites, Part A*, 2023, **169**, 107530.
11 Y. Zhang, K. Ruan and J. Gu, *Small*, 2021, **17**, 2101951.
12 L. Ma, M. Hamidinejad, B. Zhao, C. Liang and C. B. Park, *Nano–Micro Lett.*, 2022, **14**, 19.
13 M. Li, Y. Sun, D. Feng, K. Ruan, X. Liu and J. Gu, *Nano Res.*, 2023, **16**, 7820–7828.
14 D. Feng, Q. Wang, D. Xu and P. Liu, *Compos. Sci. Technol.*, 2019, **182**, 107753.
15 Z. Zeng, H. Jin, M. Chen, W. Li, L. Zhou and Z. Zhang, *Adv. Funct. Mater.*, 2016, **26**, 303–310.
16 J. Zheng, T. Hang, Z. Li, W. He, S. Jiang, X. Li, Y. Chen and Z. Wu, *Chem. Eng. J.*, 2023, **471**, 144548.
17 A. Ghaffarkhah, S. A. Hashemi, S. Rostami, M. Amini, F. Ahmadijokani, A. Pournaghshband Isfahani, S. E. Mhatre, O. J. Rojas, M. Kamkar, S. Wuttke, M. Soroush and M. Arjmand, *Adv. Funct. Mater.*, 2023, **33**, 2370294.
18 C. Li, Y. Han, Q. Du, D. Wu, J. Sun, Z. Wang and L. Zhang, *SusMat*, 2023, **3**, 345–361.
19 N. Wu, Q. Hu, R. Wei, X. Mai, N. Naik, D. Pan, Z. Guo and Z. Shi, *Carbon*, 2021, **176**, 88–105.
20 M. Wang, X. H. Tang, J. H. Cai, H. Wu, J. Bin Shen and S. Y. Guo, *Carbon*, 2021, **177**, 377–402.
21 D. Feng, P. Liu and Q. Wang, *Composites, Part A*, 2019, **124**, 105463.
22 L. C. Jia, C. G. Zhou, W. J. Sun, L. Xu, D. X. Yan and Z. M. Li, *Chem. Eng. J.*, 2020, **384**, 123368.
23 L. C. Jia, K. Q. Ding, R. J. Ma, H. L. Wang, W. J. Sun, D. X. Yan, B. Li and Z. M. Li, *Adv. Mater. Technol.*, 2019, **4**, 1800503.
24 H. Liu, S. Wu, C. You, N. Tian, Y. Li and N. Chopra, *Carbon*, 2021, **172**, 569–596.
25 Y. Bhattacharjee and S. Bose, *ACS Appl. Nano Mater.*, 2021, **4**, 949–972.
26 N. Duan, Z. Shi, J. Wang, G. Wang and X. Zhang, *Macromol. Mater. Eng.*, 2020, **305**, 1900829.
27 X. Jia, B. Shen, Z. Chen, L. Zhang and W. Zheng, *ACS Sustain. Chem. Eng.*, 2019, **7**, 18718–18725.
28 K. Chen, Y. Feng, Y. Shi, H. Wang, L. Fu, M. Liu, Y. Lv, F. Yang, B. Yu, M. Liu and P. Song, *Composites, Part A*, 2022, **160**, 107070.
29 Y. Shang, Y. Ji, J. Dong, G. Yang, X. Zhang, F. Su, Y. Feng and C. Liu, *Compos. Sci. Technol.*, 2021, **214**, 108974.
30 Y. Wang, H. K. Peng, T. T. Li, B. C. Shiu, H. T. Ren, X. Zhang, C. W. Lou and J. H. Lin, *Chem. Eng. J.*, 2021, **412**, 128681.
31 M. Ou, W. Qiu, K. Huang and S. Chu, *J. Appl. Phys.*, 2019, **125**, 134906.
32 J. Li, L. Wang, H. Luo, Q. Gao, Y. Chen, J. Xiang, J. Yan and H. Fan, *Colloids Surf., A*, 2022, **655**, 130163.
33 W. L. Song, C. Gong, H. Li, X. D. Cheng, M. Chen, X. Yuan, H. Chen, Y. Yang and D. Fang, *ACS Appl. Mater. Interfaces*, 2017, **9**, 36119–36129.
34 W. C. Yu, G. Q. Zhang, Y. H. Liu, L. Xu, D. X. Yan, H. D. Huang, J. H. Tang, J. Z. Xu and Z. M. Li, *Chem. Eng. J.*, 2019, **373**, 556–564.
35 G. Wang, X. Liao, J. Yang, W. Tang, Y. Zhang, Q. Jiang and G. Li, *Compos. Sci. Technol.*, 2019, **184**, 107847.

36 Y. J. He, Y. W. Shao, Y. Y. Xiao, J. H. Yang, X. D. Qi and Y. Wang, *ACS Appl. Mater. Interfaces*, 2022, **14**, 6057–6070.
37 X. Lu, Y. Zheng, J. Yang and J. Qu, *Composites, Part B*, 2020, **199**, 108308.
38 X. Liu, Y. Li, X. Sun, W. Tang, G. Deng, Y. Liu, Z. Song, Y. Yu, R. Yu, L. Dai and J. Shui, *Matter*, 2021, **4**, 1735–1747.
39 X. Qian, M. Ren, D. Yue, Y. Zhu, Y. Han, Z. Bian and Y. Zhao, *Appl. Catal., B*, 2017, **212**, 1–6.
40 H. Stančin, J. Růžičková, H. Mikulčić, H. Raclavská, M. Kucbel, X. Wang and N. Duić, *J. Environ. Manage.*, 2019, **243**, 105–115.
41 R. E. Salino and R. E. Catai, *Constr. Build. Mater.*, 2023, **387**, 131201.
42 Q. Wang, J. Zhang, Z. Zhou, J. Zhao, Y. Yi, S. Feng, Z. Sui, W. Zhang and C. Lu, *Small*, 2024, 2309803.
43 Y. Te Xu, Y. Wang, C. G. Zhou, W. J. Sun, K. Dai, J. H. Tang, J. Lei, D. X. Yan and Z. M. Li, *J. Mater. Chem. C*, 2020, **8**, 11546–11554.
44 X. P. Zhang, L. C. Jia, G. Zhang, D. X. Yan and Z. M. Li, *J. Mater. Chem. C*, 2018, **6**, 10760–10766.
45 Y. Han, K. Ruan and J. Gu, *Nano Res.*, 2022, **15**, 4747–4755.
46 R. Li, L. Ding, Q. Gao, H. Zhang, D. Zeng, B. Zhao, B. Fan and R. Zhang, *Chem. Eng. J.*, 2021, **415**, 128930.
47 M. Mahmoodi, M. Arjmand, U. Sundararaj and S. Park, *Carbon*, 2012, **50**, 1455–1464.
48 N. Li, Y. Huang, F. Du, X. He, X. Lin, H. Gao, Y. Ma, F. Li, Y. Chen and P. C. Eklund, *Nano Lett.*, 2006, **6**, 1141–1145.
49 L. C. Jia, D. X. Yan, X. Liu, R. Ma, H. Y. Wu and Z. M. Li, *ACS Appl. Mater. Interfaces*, 2018, **10**, 11941–11949.
50 M. Peng and F. Qin, *J. Appl. Phys.*, 2021, **130**, 225108.
51 J. Yang, X. Liao, G. Wang, J. Chen, F. Guo, W. Tang, W. Wang, Z. Yan and G. Li, *Chem. Eng. J.*, 2020, **390**, 124589.
52 X. Jia, B. Shen, L. Zhang and W. Zheng, *Carbon*, 2021, **173**, 932–940.
53 L. C. Jia, D. X. Yan, C. H. Cui, X. Ji and Z. M. Li, *Macromol. Mater. Eng.*, 2016, **301**, 1232–1241.
54 T. Kuang, L. Chang, F. Chen, Y. Sheng, D. Fu and X. Peng, *Carbon*, 2016, **105**, 305–313.
55 L. C. Jia, Y. K. Li and D. X. Yan, *Carbon*, 2017, **121**, 267–273.
56 H.-D. Huang, C.-Y. Liu, D. Zhou, X. Jiang, G.-J. Zhong, D.-X. Yan and Z.-M. Li, *J. Mater. Chem. A*, 2015, **3**, 4983–4991.
57 S. Gong, X. Sheng, X. Li, M. Sheng, H. Wu, X. Lu and J. Qu, *Adv. Funct. Mater.*, 2022, **32**, 2200570.
58 L. Ma, M. Hamidinejad, B. Zhao, C. Liang and C. B. Park, *Nano–Micro Lett.*, 2022, **14**, 19.
59 B. Xue, Y. Li, Z. Cheng, S. Yang, L. Xie, S. Qin and Q. Zheng, *Nano–Micro Lett.*, 2022, **14**, 16.
60 P. He, Z. Y. Liu, G. B. Mao, Q. Liu, M. J. Zheng, R. Z. Zuo, W. Q. Cao, Z. L. Hou, J. Yuan and M. S. Cao, *Composites, Part A*, 2022, **157**, 106935.
61 H. Zhang, Z. Heng, J. Zhou, Y. Shi, Y. Chen, H. Zou and M. Liang, *Chem. Eng. J.*, 2020, **398**, 125559.
62 C. Ma, W. T. Cao, W. Zhang, M. G. Ma, W. M. Sun, J. Zhang and F. Chen, *Chem. Eng. J.*, 2021, **403**, 126438.